

# The Effect of Interference Fit on Vibration Transmission from Stator Coil to Base of a Spindle Motor in a Hard Disk Drive

Nopdanai Ajavakom<sup>1,\*</sup> and Apirat Sillapapinij<sup>1</sup>

<sup>1</sup>Department of Mechanical Engineering, Faculty of Engineering, Chulalongkorn University, Bangkok, Thailand 10330

## Abstract

The hard disk drive spindle motor is the primary source of vibrations that cause acoustic noise in the hard disk drive (HDD). The electromagnetic forces on the stator coil and the rotor, which are inherent to the operation of motors, are responsible for the deformation causing vibration of the motor's interior structure. This vibration is transmitted to the motor exterior especially the motor base through the fit between the stator coil and the motor base. This article proposes an approach to reduce the acoustic noise of the HDD is hence by reducing the transmitted vibrational energy from the stator coil to the base by optimizing the interference fit between these two components. The effect of the fit on the transmitted vibrational energy through both the vibrational energy analysis through a friction model featuring micro-slip and the experimental investigations is studied. The vibrational energy analysis is applied on a hollow cylinder installed on a shaft as a simplified model of the stator coil and the base. The analysis shows that the transmitted torsional vibrational energy is proportional to the pressure due to the interference fit. Hence, it suggests that the reduction of the vibration transmission from the stator coil to the base can be done by decreasing the interference fit. In addition, the experimental investigations performed on three simple models of stator and base with different interference fits and also two groups of spindle motor samples with different fits agree well with the analysis.

**Keywords:** Interference fit, spindle motor, vibration transmission, statistical energy analysis

## 1. Introduction

A hard disk drive (HDD) is an important component in a personal computer to store the data. In need of higher performance HDDs including higher capacity, faster data read/write time, quieter operation while maintaining or even reducing the HDD physical size, the spindle motors are required to spin faster and smoother. Thus, the vibration transmitting from the interior to the exterior of the spindle motor, which may finally cause the data read/write errors and the emission the acoustic noise, has to be looked into. The primary source of vibration inside the motor is the electromagnetic (EM) sources, not the mechanical unbalance of the moving parts [1,2]. The EM sources are originated from the physical and the electromagnetic designs of the permanent magnet ring and the stator teeth of the motor as well as the characteristics of the input power from the motor inverter. The designs contribute the unbalance radial, tangential, and axial forces on the permanent magnet ring and the stator teeth deforming the interior structure of the motor. The deformations of the stator teeth, especially from varying tangential forces (torque ripple), are transmitted to the base bracket via the cylindrical-shell sleeve causing transverse vibration of the base plate [3]. Moreover, the deformations of the ring propagate into rotor hub as transverse and radial vibrations [3]. The vibrations of the motor exterior are responsible for the acoustic noise emitted from the motor. The approaches to decrease the vibrations and the acoustic noise from the motor include the elimination of EM sources, modification of the motor physical design to minimize the sound radiation, and reduction of the vibration transmission from the motor interior to the exterior, for example, by optimizing the interference fit between the stator coil and the base bracket. See Fig. 1.

This article focuses on the effect of interference fit between the stator coil and the base of the spindle motor on the torsional vibrational energy transmission from the stator coil to the base plate aiming to reduce the transmitted energy capable of the motor's exterior vibrations and the

emitted acoustic noise. The article presents both vibration energy transmission analysis and two experimental investigations.

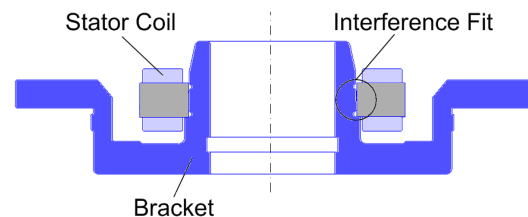


Fig. 1 Cross-section view of a spindle motor showing the fit between the stator coil and the base bracket

## 2. Vibrational Energy Transmission Analysis

The analysis of vibrational energy transmission between the stator coil and the base of the motor involves a friction model and vibration transmission mechanism of the two surfaces in contact with the clamping pressure. Jintanawan et al. [4] study a simple dynamic model of the stator coil and the base of a spindle motor featuring the two-degree of freedom lumped mass model attached to a fixed foundation via a torsional spring. The Dahl's model is used to analyze the relative angular displacement between the two components due to the applied impulsive torque at the stator coil. The study shows that the more the interference fit is, the more the vibrational energy is transmitted to the base and vice versa.

Nevertheless, for the continuous and more complex system, such as the spindle motor, the analysis that considers the internal forces on the surfaces, the micro-slip, the pre-sliding behavior, and the force's loading-unloading-reloading stages is more suitable. Such an analysis by Metherell and Diller [5] is modified to work on a stator-base model of a spindle motor. It will be shown from the hysteresis diagram of the torque versus the

\*Corresponding Author: E-mail: nopdanai.a@chula.ac.th, Tel: 02 218 6610, Fax: 02 252 2889

relative angular displacement that the vibrational energy loss is lower (the energy transmission is higher) as the interference fit is more.

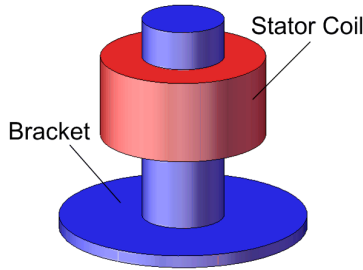


Fig. 2 Simple model of stator and base bracket

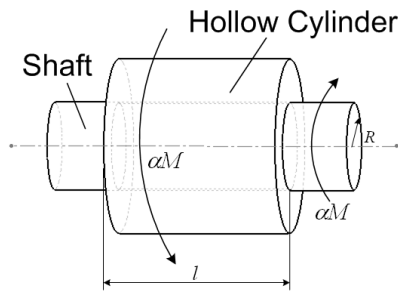


Fig. 3 Dynamic model of stator and base

Consider the simplified stator-base model shown in Fig. 2 where the stator is a ring press-fit into the base bracket via a sleeve. To simplify the analysis, the sleeve is assumed to be a solid shaft of radius  $R$  and the ring is assumed to be a hollow cylinder of length  $l$  shown in the dynamic model in Fig. 3. Torques are applied to the left side of the cylinder and the right side of the shaft. They are opposite with the equal magnitude of  $\alpha M$ , where  $0 \leq \alpha \leq 1$ , preventing any angular displacement of the whole assembly. The micro-slip is taken into account and the concept of Coulomb friction is used, the torsional friction per unit length of the cylinder on the contact surfaces is then

$$m = 2\pi\mu PR^2, \quad (1)$$

where  $m$  is the torsional friction per unit length (N-m/m),  $\mu$  is coefficient of friction,

$P$  is the pressure between the cylinder and the shaft due to the fit (Pa),

$R$  is the radius of the shaft (m). In our case, according to Eq. (1), the torsional friction per unit length is, in general, constant over the length of the cylinder due to the constant interference fit pressure, coefficient of friction and radius of the shaft. In one cycle of the varying applied torque, the torque is exerted to the model in three non-stop consecutive stages: loading, unloading, and reloading.

In the loading stage, the applied torque on the cylinder increases from 0 to  $M$ , that is  $\alpha M$ , where  $\alpha$  increases from 0 to 1. At the same time, the resisting torque at the shaft increases to balance out the applied torque creating friction on the contact surfaces. The diagrams of the torsional friction per unit length, the internal torsion on the cylinder surface, and the internal torsion on the shaft

surface are shown in Fig. 4. The torsional friction per unit length is  $m$  with the exception of being zero in the middle region of the length of the cylinder where there is no slipping. The slipping and the torsional friction occur at the left and right edge of the contact surfaces with length on each side equals  $a_1$

( $0 < a_1 < l/2$ ), where  $a_1$  depends on the magnitude of the applied torque. The internal torsion on the cylinder surface is  $\alpha M$  at the left edge and it decreases with the slope  $-m$  as it goes to the right. Likewise, the internal torsion at the shaft surface is  $\alpha M$  at the right edge and decrease with the slope  $-m$  as it goes to the left. In addition, the summation of internal torsions at the cylinder and the shaft surfaces must be equal to  $\alpha M$  along the length of the cylinder.

In the unloading stage, being reverse to the loading stage, the applied torque  $\alpha M$  on the cylinder now decreases from  $M$  to  $rM$  as  $\alpha$  decreases from 1 to  $r$ , where  $r$  is constant and  $0 \leq r < 1$ . Since the applied torque decreases, the torsional friction per unit length is now  $-m$  making the internal torsion on the cylinder surface increases with the slope  $m$  as it goes to the left. The phenomenon is called "counter slip." The counter slip occurs for the length of  $a_2$ . The further inside region of the cylinder and the shaft still experiences the torsional friction  $m$  remaining from the loading stage. The diagrams of the torsional friction per unit length, the internal torsion on the cylinder surface, and the internal torsion on the shaft surface for the unloading stage are shown in Fig. 5.

In the reloading stage, quite similar to the loading stage and reverse to the unloading stage, the applied torque  $\alpha M$  on the cylinder increases back from  $rM$  to  $M$  as  $\alpha$  increases from  $r$  to 1, where  $0 \leq r < 1$ . The torsional friction per unit length currently returns to  $m$  at the left and right sides of the cylinder. The diagrams of the torsional friction per unit length, the internal torsion on the cylinder surface, and the internal torsion on the shaft surface of the reloading stage are shown in Fig. 6.

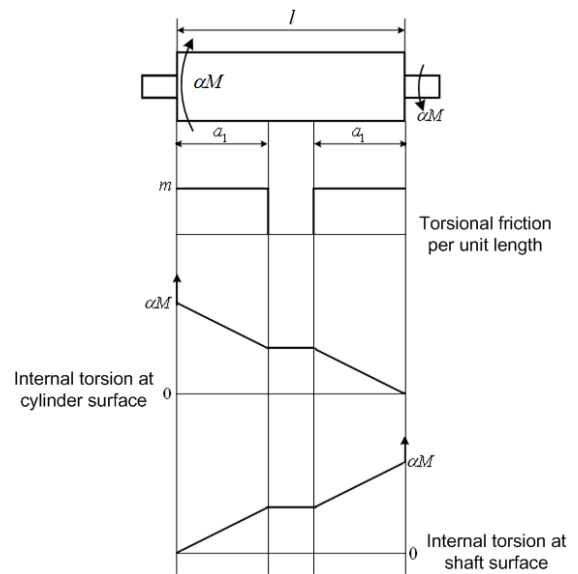


Fig. 4 Loading stage diagram

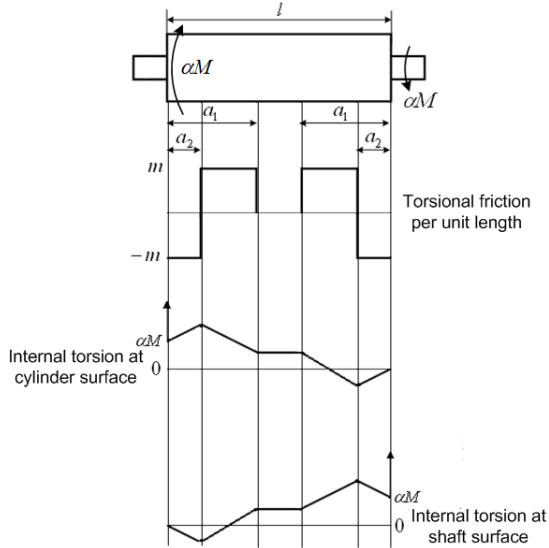


Fig. 5 Unloading stage diagram

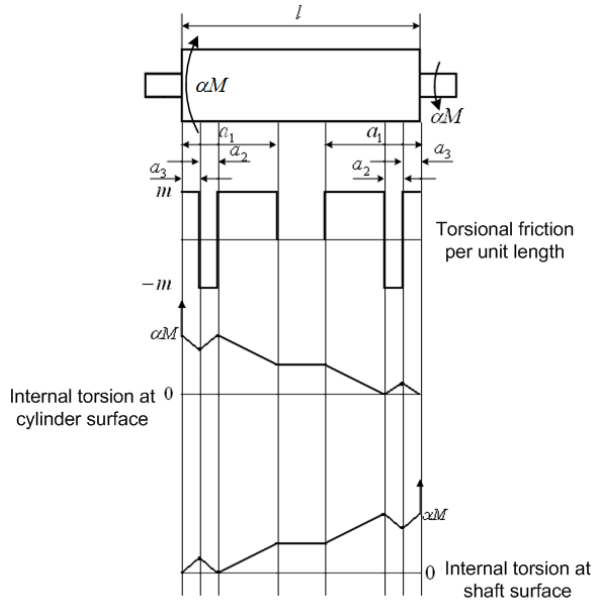


Fig. 6 Reloading stage diagram

The relative angular displacement of each stage can be determined from the torsional friction per unit length, the internal torsions on the surfaces, the shaft's and the cylinder's material properties, and other previously introduced constants:

$$\phi_1 = \frac{k\alpha M l}{G_s I_s} + \frac{(1-3k+3k^2)\alpha^2 M^2}{2mG_s I_s(1-k)}, \quad 0 < \alpha < 1 \quad (2)$$

$$\phi_2 = \frac{k\alpha M l}{G_s I_s} + \frac{M^2(1+2\alpha-\alpha^2)(1-3k+3k^2)}{4mG_s I_s(1-k)}, \quad 0 \leq r < \alpha < 1 \quad (3)$$

$$\phi_3 = \frac{k\alpha M l}{G_s I_s} + \frac{M^2(1+2r-\alpha^2-2\alpha r)(1-3k+3k^2)}{4mG_s I_s(1-k)}, \quad 0 \leq r < \alpha < 1 \quad (4)$$

$$k = \frac{G_s I_s}{G_s I_s + G_c I_c} \quad (5)$$

where  $\phi_1$ ,  $\phi_2$ ,  $\phi_3$  are the relative angular displacements for the loading, unloading, and reloading stages, respectively,  $G_c I_c$  and  $G_s I_s$  are the torsional stiffness of the cylinder and the shaft, respectively, and  $k$  is the combined torsional stiffness of the cylinder and the shaft. The angular displacements can be plotted against  $\alpha$  to form a hysteresis loop depicted in Fig. 7.

The transmission energy loss due to the friction of the fit can be obtained from the area enclosed by the relative angular displacements under the three stages over one cycle,

$$\Psi = \frac{2M_a^3(1-3k+3k^2)}{3mG_s I_s(1-k)} \quad (6)$$

where  $\Psi$  is the energy loss due to friction (J) and

$$M_a = \frac{1}{2}M(1-r), \quad 0 < r < 1 \quad (7)$$

According to Eqs. (6) and (7), the transmission energy loss depends on the cube of the applied torque and inversely depends on the torsional friction per unit length given that the other parameters are constant. Focusing on the effect of the interference fit, the equations indicate that the energy loss is less when the torsional friction is larger because of the more pressure from the tighter interference fit, Eq. (1). That is, the transmitted vibrational energy from the stator to the base would be more if the interference fit increases. This statement can also be testified by the experimental investigations in the next section.

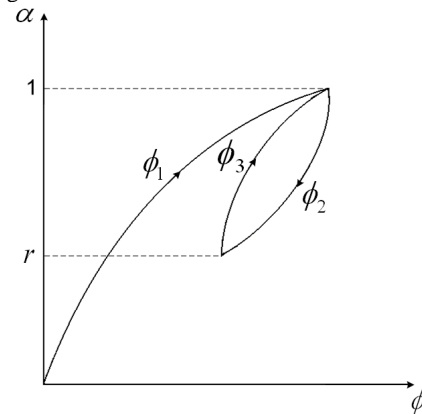


Fig. 7 Hysteresis loop of the dynamic model

### 3. Experimental Investigations

The experimental investigations are performed to testify the analytical results in the previous section. Sets of simple models of stator coil and base and 3.5-inch HDD spindle motor samples with various fits are made and tested in Sections 3.1 and 3.2, respectively. The tests were done on the simple models first and on the motor samples later.

#### 3.1 Simple models of stator coil and base

Three sets of 1.5x-size model of stator coil and base (see Fig. 8) with three interference fits, 0.0083 mm (minimum fit), 0.0169 mm (medium fit) and 0.0304 mm (maximum fit), are tested for the energy transmitted from the stator to the base. The transmission of energy between two systems, stator (system 1) and base (system 2), is analyzed by using Statistical Energy Analysis (SEA) [6, 7]. The power flow diagram is shown in Fig. 9. The input power  $P_1$  from the impact force exerted by the impact hammer at the stator model will go to raise the stator model internal energy  $W_1$ , which is related to the power loss to

the environment  $P_{11}$  and the power transmitted to the base model  $P_{12}$ . The power loss  $P_{11}$  is

$$P_{11} = \omega \eta_1 W_1, \quad (8)$$

where  $\omega$  is the frequency and  $\eta_1$  is the intrinsic loss factor. The transmitted power  $P_{12}$  is

$$P_{12} = \omega \eta_{12} W_1, \quad (9)$$

where  $\eta_{12}$  is the coupling loss factor from stator to base.

The power equation of the stator model is then

$$P_1 = P_{11} + P_{12} - P_{21}, \quad (10)$$

where  $P_{21}$  is the power received from the base. This power also depends on the base model internal energy  $W_2$  and

$$P_{21} = \omega \eta_{21} W_2, \quad (11)$$

where  $\eta_{21}$  is the coupling loss factor from base to stator.

Applying the same concept to base model where there is no direct input power from the impact hammer, the power equation of the base model is thus

$$0 = P_{22} + P_{21} - P_{12}, \quad (12)$$

where  $P_{22}$  is the power loss to the environment and

$$P_{22} = \omega \eta_2 W_2, \quad (13)$$

where  $\eta_2$  is the intrinsic loss factor of system 2.

The approach to determine the transmitted power  $P_{12}$  starts with tests to find the intrinsic loss factor of either of the two systems. The test is performed on either system separately, i.e. the stator model has not yet fit into the base model, where  $P_{12}$  and  $P_{21}$  are non-existent and

$$P_1 = P_{11} = \omega \eta_1 W_1. \quad (14)$$

The stator is then press-fit into the base. In order to simplify the testing for the power transmission, the base is damped out by attaching it to the large mass for minimizing  $W_2$  and thus  $P_{21}$  is near zero according to Eq. (11). With the known input power  $P_1$ , the intrinsic loss factors  $\eta_1, \eta_2$ , the coupling loss factor  $\eta_{12}$  as well as the transmitted power  $P_{12}$  can be calculated. With the roughly equal input power  $P_1$  of approximately  $1.11 \times 10^{-4}$  W, the transmitted power  $P_{12}$  over the 20-kHz span for all three sets with three different interference fits is shown in Fig. 10 and summarized in Table 1 with three equal ranges of frequencies. It can be observed that by roughly looking at the graph in Fig. 10 the system with the maximum interference fit has the largest transmitted power among the three systems at the frequency above 12 kHz. At the frequency below 12 kHz, the lines, however, are not smooth, which is suspected to be from some human uncertainties in the experiment, e.g. from the uneven impact force from the hammer. The numerical results for each set in the frequency ranges listed in Table 1 also indicate the similar trend. For the medium and high frequency ranges, the maximum fit set has more transmitted power than the other two sets. The medium fit set has more transmitted power than the minimum fit set. In short, generally speaking, the system with less fit possesses less transmitted power. This is consistent with the analytical results in Section 2.



Fig. 8 Assembled simple stator-base model

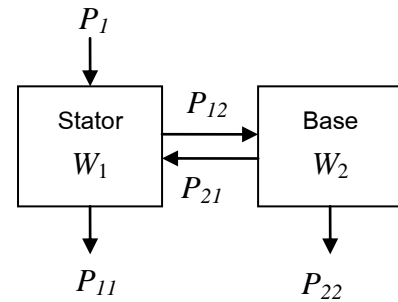


Fig. 9 Power transmission diagram of two systems

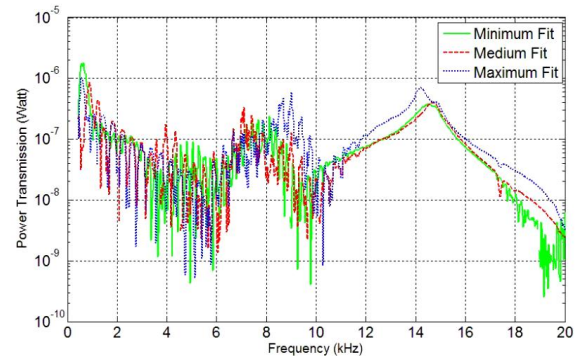


Fig. 10 Transmitted power from stator to base for three interference fits

Table 1 Power transmitted to the base with different interference fits (simple models)

Frequency range/Model fit	Transmitted power (W)		
	<i>Min</i> (8.3 $\mu\text{m}$ )	<i>Med</i> (16.9 $\mu\text{m}$ )	<i>Max</i> (30.4 $\mu\text{m}$ )
Low (0-6.6 kHz)	1.45	1.69	1.12
Medium (6.7-13.3 kHz)	1.40	1.34	2.44
High (13.4-20 kHz)	2.05	2.09	3.26
Overall (0-20 kHz)	4.90	5.12	6.82

### 3.2 3.5-inch hard disk drive spindle motors

Two groups of 3.5-inch HDD spindle motors, 3-phase permanent magnet synchronous motors (PMSMs), with different interference fits; Group A with 0.016-and 0.018-mm fits (low fit) and Group B with 0.034-mm fit (high fit), are tested to investigate the effects of stator-base interference fit on the transmitted energy. The varying frequency sinusoidal current is fed into only one phase winding of the spindle motor to excite the stator coil and the rotor structures without spinning the rotor. Particularly, the induced vibration of the stator coil is transmitted to the base plate where the transverse vibrations of 10 various points are measured for calculating the vibrational energy of the base. The transmitted vibrational energy is determined from the spatial average square velocity from the measure points and shown in joules per kg of mass per ampere of the current input in Fig. 11 over a 20-kHz span.

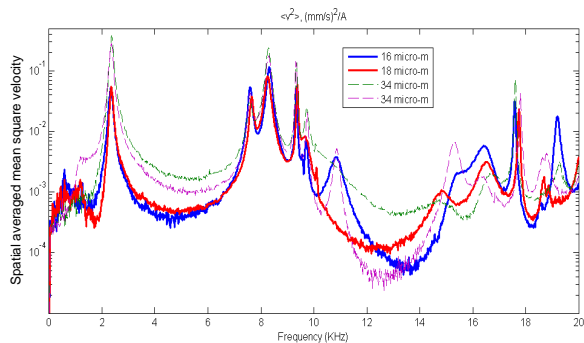


Fig. 11 Vibrational energy of spindle motors with different interference fits

The transmitted vibrational energies are also listed in Table 2 for three equal ranges of frequencies. The results indicate that the vibrational energy over the low, the medium, the high, and the overall frequency ranges of the motors with less fit (Group A) is much lower than that of the motors with more fit (Group B) especially at the low frequency range. The motors with less interference fit between the stator and the base has less transmitted vibrational energy from the stator to the base than those with more interference fit. These experimental results are consistent with those from Section 3.1 and the analytical ones in Section 2.

Table 2 Vibrational energy transmitted to the base with different interference fits (HDD spindle motors)

Frequency range/Motor group	Vibrational energy ( $\mu\text{J}/\text{kg}/\text{A}$ )	
	A (16-18 $\mu\text{m}$ )	B (34 $\mu\text{m}$ )
Low (0-6.6 kHz)	1.164	6.067
Medium (6.7-13.3 kHz)	4.063	7.263
High (13.4-20 kHz)	0.938	1.004
Overall (0-20 kHz)	6.164	14.33

### 4. Conclusion

The effect of interference fit on vibration transmission from stator coil to base of a spindle motor in a hard disk drive has been studied both analytically and experimentally. The analysis of transmission energy loss reveals that the energy loss inversely depends on the pressure from the interference fit. Less energy loss and thus

more transmitted energy from the stator to the base are the results of the more interference fit. The experimental investigations on both assembled models of the stator and the base and the spindle motor samples with various fits are carried out and their results agree well with the analysis. Hence, reducing the interference fit at the stator-base assembly in the spindle motor is a promising approach to reduce the transmitted vibrational energy to the base bracket, and the acoustic noises emitting from the motor should be lower.

### 5. References

- [1] Ajavakom, A., Jintanawan, T., Singhatanagid, P., Sripakagorn, P., 2007. On investigation of vibro-acoustics of FDB spindle motors for hard disk drives, *Microsystem Technologies*, Vol. 13, No. 8-10, pp. 1281-1287.
- [2] Lin, S., Jiang, Q., Mamun, A.A., Bi, C., 2003. Effects of drive modes on the acoustic noise of fluid dynamic bearing spindle motors. *IEEE Transactions on Magnetics*, Vol. 39, pp. 3277-3279.
- [3] Jintanawan, T., Sillapapinij, A., Ajavakom, N., 2009. Effects of tolerance design on suppression of electromagnetic-induced acoustic noises and vibration transmission in hard disk drive spindle motors. *IEEE Transactions on Magnetics*, Vol. 45, No. 11, pp. 5129-5134.
- [4] Jintanawan, T., Chungphaisan, K., Liwcharoenchai, K., Junkaew, P., Singhatanagid, P., 2007. Role of stator-base interference fit on vibration transmission and acoustic noise in FDB spindle motors for HDD. In: *Proceedings of the Information Storage Processing System Conference*.
- [5] Metherell, A.F., Diller, S.V., 1968. Instantaneous energy dissipation rate in a lap joint. *Journal of Applied Mechanics*, Vol. 35, pp. 123-128.
- [6] Lyon, R.H., 1975. *Statistical Energy Analysis of Dynamical Systems: Theory and Applications*. The MIT Press Cambridge, Massachusetts and London, England.
- [7] Sarradj, E., 2004. *Energy – based Vibroacoustics: SEA and Beyond*. Gesellschaft für Akustikforschung Dresden mbH, D-01099 Dresden, Germany.